Local Buckling Tests on Cold-Formed Steel Beams

Cheng Yu[1] and Benjamin W. Schafer[2]

Abstract: *C* and *Z* sections are two of the most common cold-formed steel shapes in use today. Accurate prediction of the bending performance of these sections is important for reliable and efficient cold-formed steel structures. Recent analytical work has highlighted discontinuities and inconsistencies in the American Iron and Steel Institute (AISI) and Canadian Standards Association (S136) design provisions for stiffened elements under a stress gradient (i.e., the web of *C* or *Z* sections). New methods have been proposed for design, and an interim method has been adopted in the North American Specification (NAS). However, existing tests on *C* and *Z* sections do not provide a definitive evaluation of the design expressions, due primarily to incomplete restriction of the distortional buckling mode. Described in this paper is a series of flexural tests with details selected specifically to insure that local buckling is free to form, but distortional buckling and lateral-torsional buckling are restricted. The members selected for the tests provide systematic variation in the web slenderness (h/t) while varying other relevant nondimensional parameters (i.e., h/b, b/t, d/t, d/b). Initial analysis of the completed testing indicates that overall test-to-predicted ratios for AISI, S136, NAS, and the direct strength method are all adequate, but systematic differences are observed.

DOI: 10.1061/(ASCE)0733-9445(2003)129:12(1596)

CE Database subject headings: Thin-wall structures; Steel beams; Buckling; Cold-formed steel.

Introduction

The determination of the ultimate bending capacity of cold-formed steel *C* and *Z* sections is complicated by yielding and the potential for local, distortional, and lateral-torsional buckling of the section, as shown in Fig. 1. Local buckling is particularly prevalent and is characterized by the relatively short-wavelength buckling of individual plate elements. Distortional buckling involves both translation and rotation at the compression flange/lip fold line of the member. The wavelength of distortional buckling is generally intermediate between that of local buckling and lateral-torsional buckling. Lateral-torsional buckling occurs when the cross section buckles without distortion.

In the process of developing the new North American Specification for the Design of Cold-Formed Steel Structural Members (NAS 2001) and harmonizing the existing American Iron and Steel Institute (AISI) (1996) and Canadian S136 (1994) methods, one of the significant differences observed between the specifications was the calculation of the web effective width. The S136 method systematically employed more conservative expressions for the web effective width. Evaluation of existing data lead to the conclusion that web/flange interaction (driven by h/b) was of primary importance (Schafer and Trestain 2002). Interim rules were adopted for NAS (2001) which use AISI (1996) when $h/b \leqslant 4$ and S136 (1994) when $h/b > 4$. However, at that time, it was felt that the issue was not fully resolved, as existing data did not distinguish between local and distortional buckling failures and was not considered to be generally representative of industry practice. Therefore, new testing and evaluation, as reported in this paper, was initiated and completed.

Existing tests on *C* and *Z* sections (see summaries by Elhouar and Murray 1985; Schafer and Peköz 1999) generally focus on the performance of the compression flange and do not provide definitive evaluations of the design expressions for the web due to: incomplete restriction of the distortional mode, arrangement of the specimens (back to back versus toe to toe), and a general lack of information on bracing details. Further, when compared with industry practice, existing data are not representative of commonly used sections. A series of new flexural tests focused on the role of web slenderness in local buckling failures of *C* and *Z* sections is reported in this paper. Bracing has been carefully considered in these tests to insure that distortional buckling and

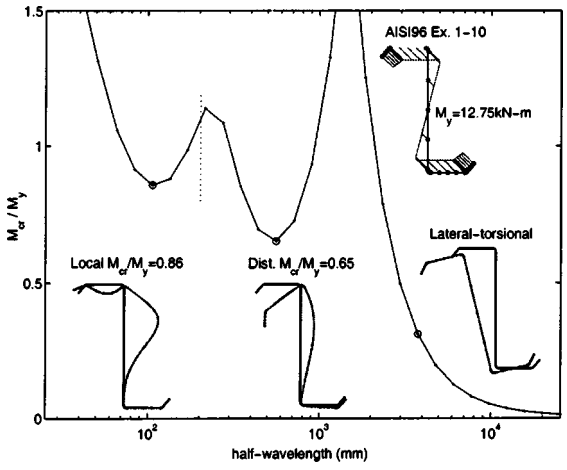

Fig. 1. Buckling modes of a cold-formed steel beam

[1]Graduate Research Assistant, 306 Latrobe Hall, Johns Hopkins Univ., Baltimore, MD 21218. E-mail: cheng.yu@jhu.edu

[2]Assistant Professor, 203 Latrobe Hall, Johns Hopkins Univ., Baltimore, MD 21218. E-mail: schafer@jhu.edu

Note. Associate Editor: Mark D. Bowman. Discussion open until May 1, 2004. Separate discussions must be submitted for individual papers. To extend the closing date by one month, a written request must be filed with the ASCE Managing Editor. The manuscript for this paper was submitted for review and possible publication on March 29, 2002; approved on March 6, 2003. This paper is part of the ***Journal of Structural Engineering***, Vol. 129, No. 12, December 1, 2003. ©ASCE, ISSN 0733-9445/2003/12-1596–1606/$18.00.

Table 1. Measured Geometry

Study No.	Test label	Specimen	h (mm)	b_c (mm)	d_c (mm)	θ_c (deg)	b_t (mm)	d_t (mm)	θ_t (deg)	r_{hc} (mm)	r_{dc} (mm)	r_{ht} (mm)	r_{dt} (mm)	t (mm)	f (MPa)
1	8.5Z120-3E2W	8.5Z120-3	214	66	24	47.2	62	25	48.9	9	9	9	9	3.00	422.65
		8.5Z120-2	215	66	24	47.8	62	25	48.9	9	9	9	9	3.00	414.09
	8.5Z105-2E1W	8.5Z105-2	215	68	24	50.5	60	24	48.7	8	8	9	9	2.64	474.03
		8.5Z105-1	214	68	25	50.7	60	23	48.7	8	8	9	9	2.67	460.25
	8.5Z092-4E2W	8.5Z092-4	214	66	24	53.0	61	24	50.8	7	7	8	8	2.29	394.80
		8.5Z092-2	214	66	23	51.8	61	24	50.4	7	7	8	8	2.25	392.64
	8.5Z082-1E2W	8.5Z082-1	215	64	24	49.0	60	25	50.3	7	7	8	8	2.03	402.38
		8.5Z082-2	215	64	24	47.9	61	24	52.4	7	7	8	8	2.04	400.34
	8.5Z073-6E5W	8.5Z073-6	216	64	23	49.6	61	24	50.9	7	7	8	8	1.83	372.20
		8.5Z073-5	216	64	23	49.6	61	24	50.9	7	7	8	8	1.85	382.97
	8.5Z073-4E3W	8.5Z073-4	216	64	24	49.6	61	23	50.3	7	7	7	7	1.82	386.85
		8.5Z073-3	216	64	23	50.1	60	24	51.0	7	7	8	8	1.83	382.76
	8.5Z073-1E2W	8.5Z073-2	216	65	24	50.2	61	23	51.0	7	7	8	8	1.82	383.49
		8.5Z073-1	216	64	23	48.4	61	24	51.2	7	7	8	8	1.83	377.41
	8.5Z065-3E1W	8.5Z065-3	215	61	21	47.3	62	20	47.3	7	7	7	7	1.63	368.62
		8.5Z065-1	215	62	19	47.4	62	21	47.1	7	7	7	7	1.63	365.86
	8.5Z059-4E3W	8.5Z059-4	216	64	20	50.9	60	18	48.9	7	7	7	7	1.50	403.75
		8.5Z059-3	216	62	20	50.2	56	18	50.4	7	7	7	7	1.51	403.07
	8.5Z059-2E1W	8.5Z059-2	216	64	20	50.6	59	18	50.2	7	7	7	7	1.50	407.20
		8.5Z059-1	216	64	20	51.2	59	18	49.4	7	7	7	7	1.50	405.82
2	11.5Z092-1E2W	11.5Z092-1	290	85	24	50.1	89	24	49.5	6	7	7	7	2.61	420.43
		11.5Z092-2	288	84	25	48.3	90	23	48.1	7	7	7	7	2.62	416.29
	11.5Z082-2E1W	11.5Z082-2	291	89	22	50.3	88	22	52.2	8	8	9	9	2.13	423.65
		11.5Z082-1	291	89	23	50.6	87	22	51.0	8	8	9	9	2.13	416.36
	11.5Z073-2E1W	11.5Z073-2	289	89	22	46.0	85	21	44.8	7	7	7	7	1.80	450.61
		11.5Z073-1	288	89	24	45.4	86	23	44.2	7	3	7	2	1.77	460.39
3	8C097-2E3W	8C097-2	204	54	15	85.6	53	13	85.7	8	7	7	8	2.49	412.71
		8C097-3	204	53	14	84.0	53	14	88.2	8	7	7	7	2.39	410.64
	8C068-4E5W	8C068-4	204	52	13	83.2	52	13	87.0	7	6	6	6	1.91	334.85
		8C068-5	203	52	13	84.0	52	14	87.6	7	6	6	7	1.96	365.86
	8C068-1E2W	8C068-2	204	52	13	83.4	52	14	87.6	7	6	6	7	1.93	356.21
		8C068-1	204	52	14	83.1	52	13	88.1	8	6	6	7	1.92	354.15
	8C054-1E8W	8C054-1	203	52	13	88.9	53	13	84.7	6	6	6	6	1.40	275.60
		8C054-8	205	51	15	88.1	50	12	82.3	6	5	6	6	1.37	277.67
	8C043-5E6W	8C043-5	204	51	14	88.8	50	14	87.3	5	5	5	5	1.26	309.36
		8C043-6	205	51	14	88.9	51	12	87.0	5	5	6	5	1.24	310.05
	8C043-3E1W	8C043-3	204	51	14	89.3	51	13	87.5	5	5	5	5	1.20	316.94
		8C043-1	204	51	14	89.0	50	14	85.8	5	5	7	5	1.21	314.87
4	12C068-9E5W	12C068-9	305	49	13	82.0	51	14	85.3	7	7	8	7	1.66	241.70
		12C068-5	305	45	14	85.9	52	14	94.8	7	7	6	7	1.66	240.87
	12C068-3E4W	12C068-3	304	50	15	82.5	51	14	77.4	6	7	7	7	1.70	390.25
		12C068-4	305	51	13	80.6	51	13	83.3	7	7	7	7	1.70	394.66
	10C068-2E1W	10C068-2	256	49	13	83.2	50	13	83.3	7	6	7	6	1.45	231.23
		10C068-1	255	52	14	80.7	50	14	81.9	7	7	7	6	1.45	235.57
	6C054-2E1W	6C054-2	153	51	14	85.7	51	13	90.0	5	6	7	6	1.56	248.73
		6C054-1	153	51	14	86.5	52	13	90.5	6	6	6	6	1.57	254.64
	4C054-1E2W	4C054-1	100	51	14	79.2	51	14	77.4	6	6	6	6	1.40	309.85
		4C054-2	100	49	13	74.2	50	14	74.8	6	7	6	6	1.42	308.06
	3.62C054-1E2W	3.62C054-1	93	50	12	77.1	51	11	88.1	6	7	7	6	1.41	225.79
		3.62C054-2	93	50	13	79.8	50	11	79.8	6	6	6	7	1.41	220.37

Note: Typical specimen label is $\times Z$(or C)xxx-x. For example, 8.5Z073-1 means the specimen is 216 mm (8.5 in.) high for the web, Z section, 1.85 mm (0.073 in.) thick and the beam number is 1 (used to distinguish with other specimens with same dimensions). Typical test label is $\times Z$(or C)xxx-xExW. For example, test 8.5Z073-1E2W means the two paired specimens are 8.5Z073-1 at the east side and 8.5Z073-2 at the west side.

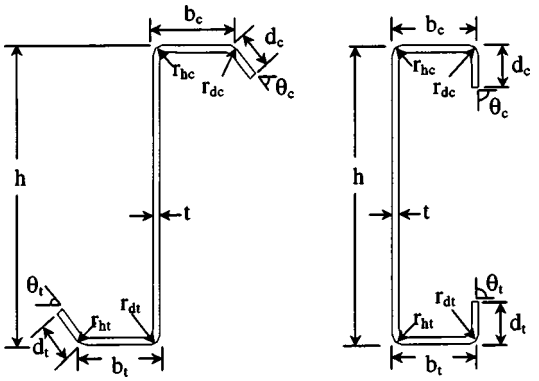

Fig. 2. Definitions of specimen dimensions for *Z* and *C*

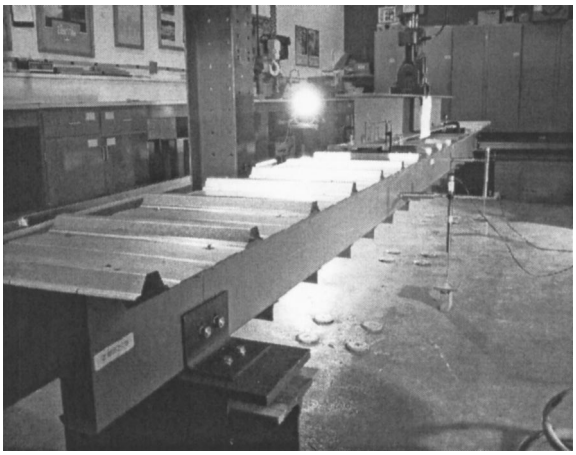

Fig. 4. Overall view of test setup

lateral-torsional buckling do not influence the interpretation of results. The test results can be used for the evaluation of existing and proposed methods for strength prediction of webs in local buckling. In addition, these tests can form the basis for later evaluations in which restrictions on the distortional mode are relieved.

Local Buckling Tests

Specimen Selection

The AISI (1996) specification calculates the effective width of webs as a function of the web slenderness (h/t) alone. The proposed tests are designed to provide systematic variation in web slenderness (h/t) while also varying the other nondimensional parameters that govern the problem such as flange slenderness (b/t), edge stiffener slenderness (d/t), and relevant interactions, such as the web height to flange width (h/b) ratio. The focus of the testing is on the web, therefore significant variation in stiffener length to flange width ratio (d/b) is not investigated.

The selected specimens are summarized in Table 1. The use of industry standard sections dictates the manner in which the web slenderness (h/t) can be varied. For the *Z* sections, the specimens vary in *t* while holding *h*, *b*, and *d* approximately constant (studies 1 and 2 in Table 1). However, the wide variety of *C* specimens commonly produced to the Steel Stud Manufacturers Association Standards allows both independent *h* and *t* variations to be examined for *C* sections (studies 3 and 4 in Table 1).

The dimensions of the specimens were recorded at midlength and middistance between the center and loading points, for a total of three measurement locations for each specimen. The definitions of specimen dimensions for *Z* and *C* are shown in Fig. 2. The mean dimensions, as determined from the three sets of measurements within the constant moment region, are given in Table 1.

Testing Details

The basic testing setup is illustrated in Figs. 3–6. The 4.9 m (16 ft) span length, four-point bending test, consists of a pair of 5.5 m (18 ft) long *C* or *Z* specimens in parallel loaded at the 1/3 points. The members are oriented in an opposed fashion, such that in-plane rotation of the *C* or *Z* leads to tension in the panel, and thus provides additional restriction against distortional buckling of the compression flange. Small angles, $32\times32\times1.45$ mm (1 1/4 $\times$1 1/4$\times$0.057 in.), are attached to the tension flanges every 305 mm (12 in.) and a through-fastened panel [$t=0.48$ mm (0.019 in.), 32 mm (1 1/4 in.) high rib] is attached to the compression flanges. Hot-rolled tube sections, $254\times191\times152\times6$ mm (10×7 1/2$\times6\times$1/4 in.), bolt the pair of *C* or *Z* sections together at the load points and the supports, and insure that shear and web crippling problems are avoided at these locations. When testing the *Z*'s, the hot-rolled angles detailed at the end plates (Fig. 4) connect to the tube and the purlin to remove any crippling or rolling at the supports. The *C*'s use a similar detail, but the connection is to the inside of the tube.

The loading system employs an 89 kN (20 kip) MTS actuator, which has a maximum 152 mm (6 in.) stroke. The test was performed in displacement control at a rate of 0.0381 mm/s (0.0015 in./s). An MTS 407 controller and load cell monitored the force and insured the desired displacement control was met. Meanwhile, deflections for one specimen at the 1/3 points were measured using two linear variable differential transformers (LVDTs).

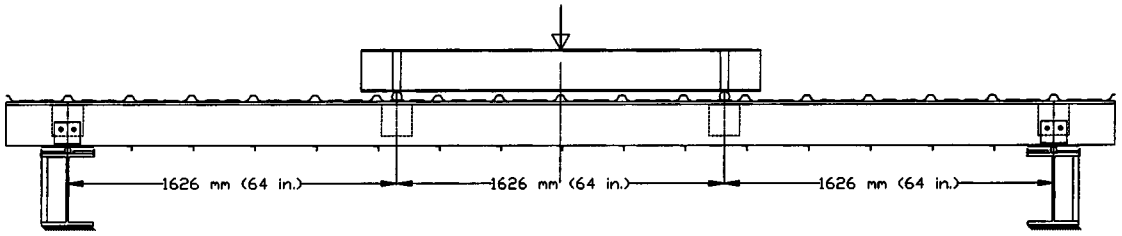

Fig. 3. Elevation view of overall test arrangement for four point bending test

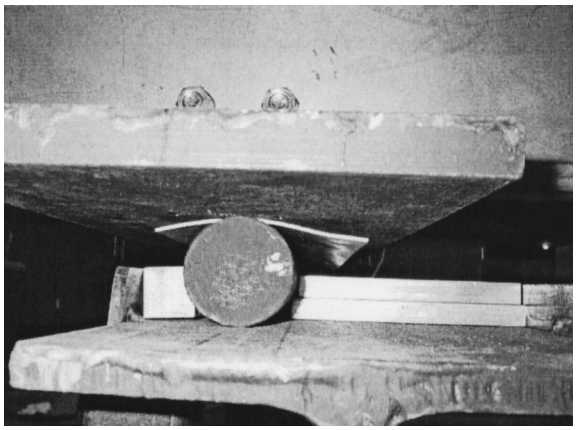

Fig. 5. Support configuration

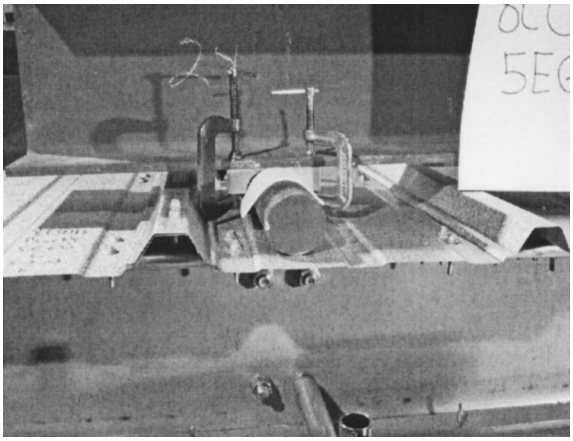

Fig. 6. Loading point configuration

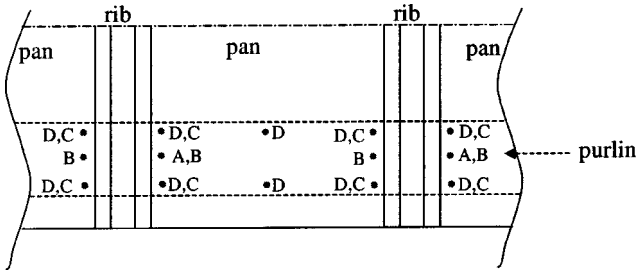

Fig. 7. Plan view of fastener locations for panel-to-purlin connection

Later, for the 254 mm (10 in.) *C* and 292 mm (11.5 in.) *Z* beams, the 2 LVDTs were replaced by four position transducers. For a limited number of tests, strain gauges were placed at midspan, on the lip, and the top of the web, at the same vertical cross section height, to monitor the longitudinal strain.

After initial testing, the details were improved to insure pure bending was maintained, and to restrict distortional and lateral-torsional buckling. The arrangement of rollers at the supports was modified to more closely model a pin-roller configuration (Fig. 5). Additional web stiffening bars were added to the I beams at the supports and load points. Machined, quarter-round aluminum blocks were placed as guides for the rollers at the loading points (Fig. 6). Thin Teflon sheets were added at the load points and support points to limit unwanted friction and help insure that the boundary conditions were predictable (Figs. 5 and 6).

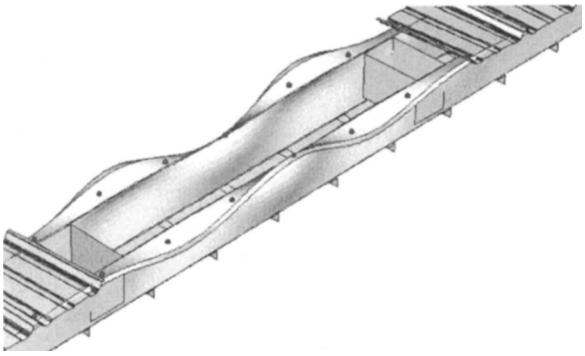

Fig. 8. Lowest buckling mode predicted by finite element model for single screw fastener configuration (note center panels removed for visual clarity only, the dots indicate fastener locations)

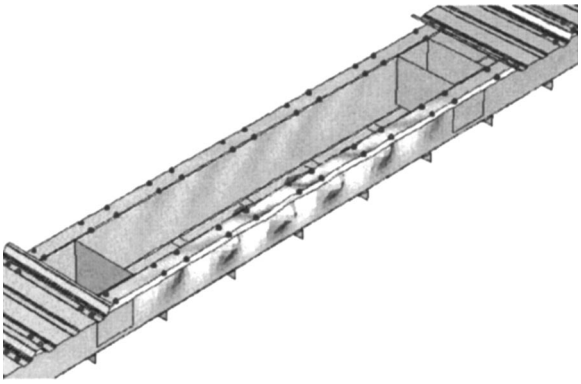

Fig. 9. Lowest buckling mode predicted by finite element model for paired screw fastener configuration (note center panels removed for visual clarity only, the dots indicate fastener locations)

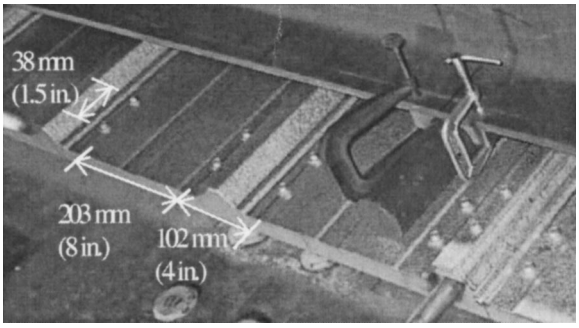

Fig. 10. Selected standard panel-to-purlin and panel-to-panel fastener configuration

Panel-to-Purlin Fastener Configuration

A series of tests on the 216 mm (8.5 in.) deep *Z*'s with $t = 1.85$ mm (0.073 in.) and $t = 1.50$ mm (0.059 in.) was conducted in order to determine the appropriate panel-to-purlin fastener detail for restricting the distortional mode. Investigated fastener locations are depicted in Fig. 7. Initial testing using single panel-to-purlin fasteners placed through the center of the purlin flange and spaced at 305 mm (12 in.) on center (test 8.5Z073-6E5W, panel type A) failed at a capacity of 89% of the AISI (1996) prediction and visually appeared to suffer from deformations consistent with distortional buckling. Elastic finite element analysis,

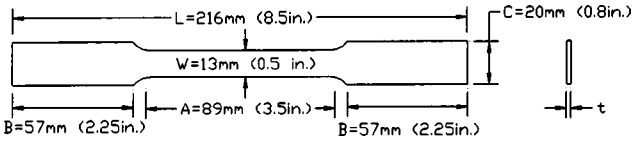

Fig. 11. Dimensions of tensile coupon

Fig. 8, using the commercial finite element package *ABAQUS* (HKS 2001) confirmed that the lowest elastic buckling mode for this fastener detail was distortional buckling. Additional analysis (Fig. 9) indicated that a pair of fasteners placed on either side of the raised ribs (panel type C) would force local buckling to be the lowest mode. Testing of 8.5Z073-4E3W confirmed this prediction and paired fasteners as shown in Fig. 10 provided a capacity 10% greater than single fasteners and 98% of the AISI (1996) prediction. Further, testing (8.5Z059-2E1W) with additional paired fasteners in the center of the pans (Fig. 7, panel type D) did not improve the results over type C (compare with test 8.5Z059-4E3W). Additionally, the modeling indicates that the paired fasteners do not change the local buckling mode; thus, it can be safely assumed that panel type C restricts distortional buckling without artificially increasing the local buckling strength.

The selected standard panel-to-purlin fastener detail (panel type C) for this study is a pair of screws placed 38 mm (1.5 in.) for *C* section, 64 mm (2.5 in.) for *Z* section, apart and spaced 203 mm (8 in.) away from a second pair in the pan of the deck, as shown in Fig. 10. The paired fastener configuration is only maintained inside the constant moment region of the test. In the shear span, one screw is used instead of one pair, at the same location as that of the constant moment region.

Tension Tests

Tension tests were carried out following ''ASTM E8-00 Standard Test Methods for Tension Testing of Metallic Material'' (ASTM 2000). The dimensions of a typical tensile coupon are shown in Fig. 11 and the test results are given in Table 2. Three tensile coupons were taken from the end of each specimen: one from the web flat, one from the compression flange flat, and one from the tension flange flat, average results are given in Table 2. A screw-driven ATS 900, with a maximum capacity of 44.5 kN (10 kips) was used for the loading. An MTS 634.11E-54 extensometer was employed to monitor the deformation. Strain gauges were installed on selected tensile coupons at the center, and on both sides, to verify the modulus of elasticity, *E*. Two methods for yield strength determination were employed: (1) 0.2% offset method for the continuous yielding materials [Fig. 12(a)]; and (2) autographic diagram method for the materials exhibiting discontinuous yielding [Fig. 12(b)].

The yield stress (f_y) can vary greatly across the test series. The large variation in f_y complicates comparisons across the test database, but it is important to recognize this variation, as f_y for the *Z*'s varied from 365 to 475 MPa (53 to 69 ksi) and for the *C*'s from 220 to 413 MPa (32 to 60 ksi). An *E* of 203 MPa (29,500 ksi) is assumed for all of the members. This is supported by limited testing on 1.5 mm (0.059 in.) and 2.08 mm (0.082 in.) tensile specimens from the *Z*'s, which had an average measured *E* of 201 MPa (29,200 ksi).

Experimental Results

A summary of the local buckling test results is given in Table 3. Included for each test are the elastic buckling moments (M_{cr}) as

Table 2. Summary of Tension Test Results

Specimen	t (mm)	f_y (MPa)	f_u (MPa)	f_u/f_y ratio (%)
Panel2	0.465	693.9	699.6	101
Panel1	0.462	697.6	718.0	103
8.5Z120-3	3.005	422.7	580.6	137
8.5Z120-2	2.987	413.8	568.9	137
8.5Z105-2	2.635	474.3	629.0	133
8.5Z105-1	2.661	460.6	614.1	133
8.5Z092-4	2.287	395.2	498.1	126
8.5Z092-2	2.263	392.6	495.4	126
8.5Z082-2	2.041	400.3	510.2	127
8.5Z082-1	2.048	402.2	509.9	127
8.5Z073-6	1.829	372.2	500.4	134
8.5Z073-5	1.847	383.0	507.2	132
8.5Z073-4	1.815	386.9	514.6	133
8.5Z073-3	1.829	382.8	512.1	134
8.5Z073-2	1.829	377.4	504.0	134
8.5Z073-1	1.816	383.5	510.3	133
8.5Z065-3	1.635	368.8	474.4	129
8.5Z065-1	1.631	365.7	472.5	129
8.5Z059-4	1.511	404.0	557.3	138
8.5Z059-3	1.512	402.8	558.3	139
8.5Z059-2	1.499	407.2	556.9	137
8.5Z059-1	1.499	405.8	555.2	137
11.5Z092-2	2.625	416.3	537.4	129
11.5Z092-1	2.609	420.4	541.1	129
11.5Z082-2	2.126	423.7	558.1	132
11.5Z082-1	2.130	416.4	550.7	132
11.5Z073-2	1.800	450.6	570.7	127
11.5Z073-1	1.766	460.4	582.5	127
8*C*097-3	2.378	410.9	524.4	128
8*C*097-2	2.483	412.7	528.4	128
8*C*068-5	1.917	334.7	444.9	133
8*C*068-4	1.950	365.6	456.5	125
8*C*068-2	1.914	354.3	454.4	128
8*C*068-1	1.923	356.5	450.2	126
8*C*054-8	1.371	278.0	363.5	131
8*C*054-4	1.501	321.1	420.0	131
8*C*054-1	1.385	275.9	358.6	130
8*C*043-6	1.248	310.3	418.8	135
8*C*043-5	1.260	309.1	420.1	136
8*C*043-3	1.198	316.6	423.6	134
8*C*043-1	1.207	314.7	422.6	134
6*C*054-2	1.564	248.7	346.8	139
6*C*054-1	1.565	254.6	344.5	135
4*C*054-2	1.424	308.1	375.8	122
4*C*054-1	1.399	309.9	382.3	123
3.62*C*054-2	1.406	220.4	372.8	169
3.62*C*054-1	1.410	225.8	371.5	165
12*C*068-9	1.657	241.7	403.1	167
12*C*068-5	1.662	240.2	403.9	168
12*C*068-4	1.701	394.7	523.2	133
12*C*068-3	1.704	390.2	516.1	132
10*C*068-2	1.453	231.3	394.9	171
10*C*068-1	1.455	235.6	392.2	167

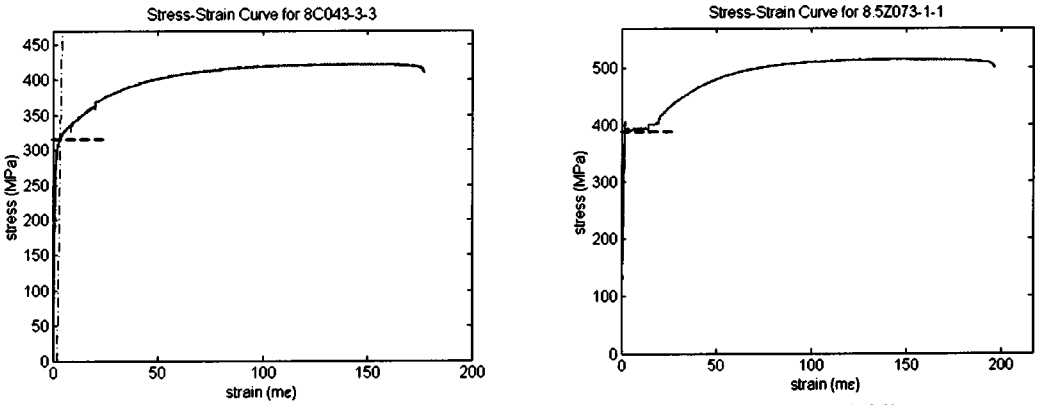

(a) Continuous yielding curve

(b) Discontinuous yielding curve

Fig. 12. Typical stress–strain curve of tension test

determined by the finite strip method using *CUFSM* (Schafer 2001) and ratios of test-to-predicted capacities for various design methods.

Strain gauges were placed at midspan, on the lip and the top of the web, at the same vertical cross section height, on nine *C* members (footnote c in Table 3), to monitor the longitudinal strain. Typical output from the gauges is given in Fig. 13. In the initial elastic range, the gauges read nearly identical and agree with the simple beam theory predictions, indicating that the testing arrangement is achieving the desired loading about the geometric axis and no twisting is developing in the section. At an intermediate load level, before buckling deformations were visible, strain on either the lip or web began to reverse. In most, but not all, the strain on the lip began to reverse prior to the web. Once buckling initiates the strain distribution varies around the profile and along the length, and it becomes difficult to provide definitive conclusions from the limited strain data.

The actuator load–displacement response is given in Figs. 14–17. Little nonlinear response is observed prior to formation of the failure mechanism. The specimens which have a tested capacity at or near the yield moment ($M_{\text{test}}/M_y \sim 1$, see Table 3) exhibit the most nonlinear deformation prior to failure; while the more slender specimens have essentially elastic response prior to formation of a sudden failure mechanism.

As shown in Figs. 14–17 failure of the weaker specimen of the pair results in a significant loss in capacity. The redistribution of load into the second specimen of the pair causes complete failure soon thereafter. Failure of the second specimen can be recognized by the change in slope of the postpeak load-deformation response. In the studied members, the postpeak response of the *C*'s was generally more gradual than comparable *Z*'s, even in the thinner specimens. In tests on the *C*'s, both specimens tend to fail at approximately the same time, as opposed to the progressive failure observed in most tests on *Z*'s. The observed failure mechanisms for the *C*'s are shown in Fig. 18 (see Fig. 19 for the *Z*'s).

Comparison with Design Methods

Four design methods were considered for comparison: The existing American Specification (AISI 1996), the existing Canadian Standard (S136 1994), the newly adopted combined U.S./Canada/Mexico–North American Specification (NAS 2001) and the recently proposed direct strength method (Schafer and Peköz 1998; Schafer 2002a,b). For flexural capacity, the AISI and S136 methods are essentially identical except for the expressions for the effective width of the web. The S136 method assumes the web is partially effective for $\lambda_{\text{web}} > 0.673$ while the AISI method does not. The NAS method is a combination of AISI and S136, when $h/b \leq 4$, the AISI method is used, when $h/b > 4$ the S136 method is used.

Test-to-Predicted

Test-to-predicted ratios for the considered design methods are provided for all specimens in Table 3 and depicted graphically as a function of web slenderness in Fig. 20. As shown in Table 4 and Fig. 20, the AISI method either predicts the same strength as the S136 method (in the case of fully effective sections) or systematically predicts higher strengths. The difference between the AISI and S136 method is greatest for intermediate web slenderness values, $1.0 \leq \lambda_{\text{web}} \leq 1.5$. For the majority of the tested members, h/b is less than 4, therefore NAS and AISI are essentially the same; however, for a few of the deeper *C* sections, 254 mm (10 in.) deep and 305 mm (12 in.) deep h/b is greater than 4 and thus NAS results match those of S136.

On average, as summarized in Table 4, AISI, S136, and NAS provide adequate strength prediction. The average AISI test-to-predicted ratio is actually 1.01, indicating remarkably good agreement. However, this can be misleading—the maximum predicted capacity for these members is the yield moment (M_y) but several of the specimens (denoted as nonslender) experienced inelastic reserve capacity with $M_{\text{test}}/M_y > 1.0$. As a result, all of the unslender members have quite conservative test-to-predicted ratios; this brings the overall averages up, even though the average test-to-predicted ratio for slender members is slightly less than 1.0. Individual AISI test-to-predicted ratios for slender members are observed to be as low as 0.86. For S136, the results are systematically more conservative, while the NAS results are essentially identical to AISI with the exception of the deeper *C* sections noted above.

The direct strength method provides separate strength predictions for local and distortional buckling. The high test-to-predicted ratios for distortional buckling ($M_{\text{test}}/M_{\text{DSd}}$) indicate that distortional buckling is successfully restricted with the testing details employed. However, the low strength predictions for M_{DSd} indicate that if the beam did not have a panel restricting the flange movement, the observed capacity would be considerably less due to a tendency to fail in distortional buckling. The overall agree-

Table 3. Local Buckling Test Results

Test label	Panel type[d]	Specimen	M_{test} (kN m)	M_y (kN m)	M_{crl} (kN m)	M_{crd} (kN m)	M_{test}/M_y	M_{test}/M_{AISI}	M_{test}/M_{S136}	M_{test}/M_{NAS01}	M_{test}/M_{DSl}	M_{test}/M_{DSd}
8.5Z120-3E2W	C	8.5Z120-3	31.7	30.3	82.2	44.2	1.05	1.05	1.05	1.05	1.05	1.22
		8.5Z120-2[b]	31.7	29.8	81.6	44.2	1.06	1.06	1.06	1.06	1.06	1.23
8.5Z105-2E1W	C	8.5Z105-2	30.2	30.5	54.3	33.1	0.99	1.05	1.07	1.04	0.99	1.28
		8.5Z105-1[b]	30.2	29.9	55.0	33.3	1.01	1.06	1.07	1.06	1.01	1.29
8.5Z092-4E2W	C	8.5Z092-4	20.5	21.7	36.3	24.5	0.94	0.98	1.01	0.98	0.94	1.20
		8.5Z092-2[b]	20.5	21.4	34.6	23.5	0.96	1.01	1.04	1.01	0.97	1.23
8.5Z082-1E2W	C	8.5Z082-1[b]	18.3	19.6	25.5	19.3	0.93	1.00	1.05	1.00	1.01	1.25
		8.5Z082-2	18.3	19.6	25.9	19.7	0.93	1.00	1.05	0.99	1.00	1.24
8.5Z073-6E5W	A	8.5Z073-6[b]	13.7	16.5	18.7	15.1	0.83	0.92	0.99	0.91	0.94	1.15
		8.5Z073-5	13.7	17.1	19.2	15.4	0.80	0.89	0.96	0.88	0.91	1.11
8.5Z073-4E3W	C	8.5Z073-4	15.1	17.1	18.2	14.6	0.88	0.98	1.06	0.98	1.02	1.26
		8.5Z073-3[b]	15.1	17.0	18.7	15.3	0.89	1.00	1.08	0.99	1.01	1.24
8.5Z073-1E2W	B	8.5Z073-2[b]	13.9	17.0	18.2	14.7	0.82	0.91	0.98	0.91	0.94	1.16
		8.5Z073-1	13.9	16.7	18.8	15.2	0.84	0.92	0.99	0.92	0.94	1.16
8.5Z065-3E1W	C	8.5Z065-3	10.8	14.1	13.0	10.1	0.77	0.86	0.96	0.86	0.93	1.18
		8.5Z065-1[b]	10.8	13.9	13.2	10.4	0.78	0.89	0.99	0.89	0.93	1.17
8.5Z059-4E3W	C	8.5Z059-4[b]	11.4	14.3	9.8	8.3	0.79	0.98	1.07	0.98	1.06	1.34
		8.5Z059-3	11.4	14.1	9.7	8.6	0.80	0.97	1.06	0.97	1.07	1.33
8.5Z059-2E1W	D	8.5Z059-2	11.2	14.4	9.7	8.3	0.78	0.96	1.04	0.96	1.04	1.32
		8.5Z059-1[b]	11.2	14.4	9.7	8.3	0.78	0.96	1.04	0.96	1.04	1.32
11.5Z092-1E2W[a]	C	11.5Z092-1	39.8	46.8	53.6	13.1	0.85	0.99	1.10	0.99	0.96	1.30
		11.5Z092-2[b]	39.8	46.2	54.0	13.8	0.86	1.00	1.10	1.00	0.96	1.34
11.5Z082-2E1W	C	11.5Z082-2[b]	31.0	39.0	28.5	13.7	0.79	1.05	1.13	1.05	1.04	1.38
		11.5Z082-1	31.0	38.5	28.6	14.8	0.80	1.04	1.13	1.04	1.04	1.39
11.5Z073-2E1W	C	11.5Z073-2[b]	21.9	35.2	17.0	13.1	0.62	0.96	1.01	0.96	0.94	1.31
		11.5Z073-1[c]	21.9	35.6	16.3	13.8	0.62	0.96	1.00	0.96	0.95	1.30
8*C*097-2E3W	C	8*C*097-2[c]	19.5	18.7	37.8	27.3	1.04	1.07	1.08	1.07	1.04	1.21
		8*C*097-3[b]	19.5	17.8	34.9	25.6	1.10	1.13	1.15	1.13	1.10	1.28
8*C*068-4E5W	C	8*C*068-4[c]	11.7	11.5	18.3	15.4	1.02	1.05	1.10	1.05	1.03	1.22
		8*C*068-5[b]	11.7	12.9	19.9	16.5	0.91	0.95	0.99	0.95	0.93	1.10
8*C*068-1E2W	C	8*C*068-2[b]	11.1	12.3	18.8	15.7	0.90	0.94	0.98	0.94	0.93	1.10
		8*C*068-1	11.1	12.2	18.6	15.5	0.91	0.94	0.98	0.94	0.94	1.11
8*C*054-1E8W	C	8*C*054-1[b,c]	6.3	7.0	7.4	7.4	0.90	0.97	1.07	0.95	1.04	1.17
		8*C*054-8	6.3	7.1	6.7	6.9	0.89	0.93	1.02	0.93	1.07	1.20
8*C*043-5E6W	C	8*C*043-5	5.8	7.2	5.3	5.8	0.80	0.95	1.04	0.95	1.05	1.17
		8*C*043-6[b]	5.8	7.1	5.0	5.4	0.81	0.96	1.06	1.06	1.07	1.21
8*C*043-3E1W	C	8*C*043-3	5.4	7.1	4.7	5.1	0.76	0.93	1.01	0.93	1.03	1.17
		8*C*043-1[b,c]	5.4	7.0	4.7	5.1	0.77	0.93	1.01	0.93	1.04	1.17
12*C*068-9E5W	C	12*C*068-9[b]	11.8	12.8	9.9	13.1	0.92	0.95	1.08	1.08	1.18	1.32
		12*C*068-5[c]	11.8	12.4	10.1	13.8	0.95	0.98	1.12	1.12	1.19	1.33
12*C*068-3E4W	C	12*C*068-3	15.5	21.5	10.9	14.8	0.72	0.86	0.93	0.93	1.07	1.25
		12*C*068-4[b]	15.5	21.8	10.6	13.7	0.71	0.90	0.97	0.95	1.07	1.28
10*C*068-2E1W	C	10*C*068-2	7.9	8.3	7.3	13.7	0.96	0.98	1.11	1.11	1.18	1.28
		10*C*068-1[b]	7.9	8.6	7.3	14.8	0.92	0.94	1.06	1.06	1.14	1.23
6*C*054-2E1W	C	6*C*054-2[b,c]	5.1	4.8	11.4	9.9	1.06	1.09	1.09	1.09	1.06	1.16
		6*C*054-1	5.1	4.9	11.6	9.2	1.04	1.06	1.06	1.06	1.04	1.14
4*C*054-1E2W	D	4*C*054-1	3.1	3.1	7.5	4.9	1.02	1.11	1.11	1.10	1.02	1.15
		4*C*054-2[b,c]	3.1	3.0	8.3	5.1	1.03	1.13	1.13	1.11	1.03	1.15
3.62*C*054-1E2W	D	3.62*C*054-1[b,c]	2.3	2.0	7.2	4.3	1.16	1.20	1.20	1.20	1.16	1.24
		3.62*C*054-2	2.3	2.0	7.3	4.6	1.17	1.20	1.20	1.20	1.17	1.24

[a]Result is estimated as peak load exceeds the recording range.

[b]Controlling specimen, weaker capacity by AISI (1996).

[c]Strain gauges were placed at midspan, on the lip and the top of the web, at the same vertical cross-section height.

[d]Panel fastener type, see details in Fig. 7.

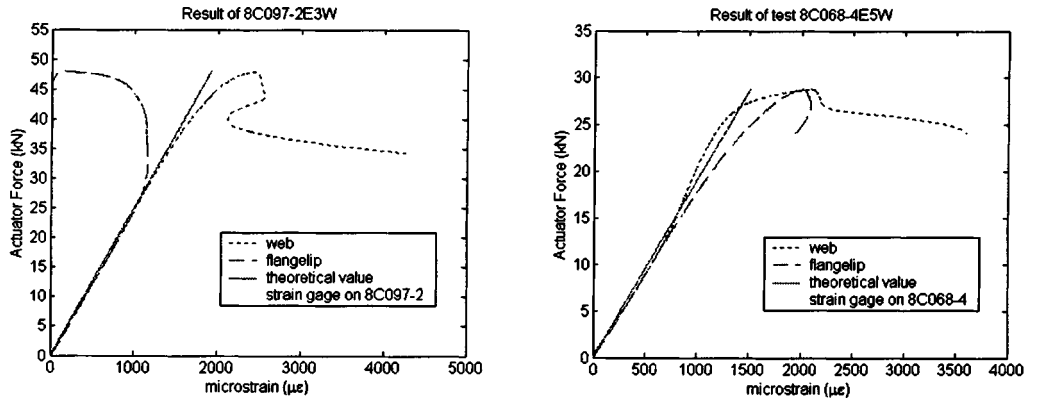

(a) t=2.46 mm (test 8C097-2E3W) first failure occurred in this specimen near the strain gages

(b) t=1.73 mm (test 8C068-4E5W) first failure occurred in the other beam of the pair

Fig. 13. Strain on web and lip for tests on 203 mm (8 in.) nominal deep *C*'s

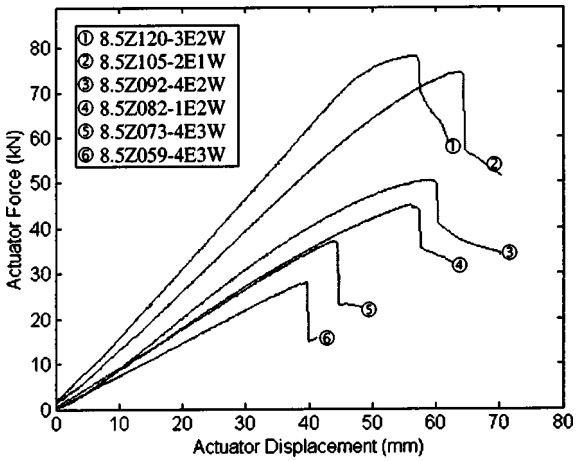

Fig. 14. Actuator force–displacement response for tests of 216 mm (8.5 in.) nominal deep *Z*'s

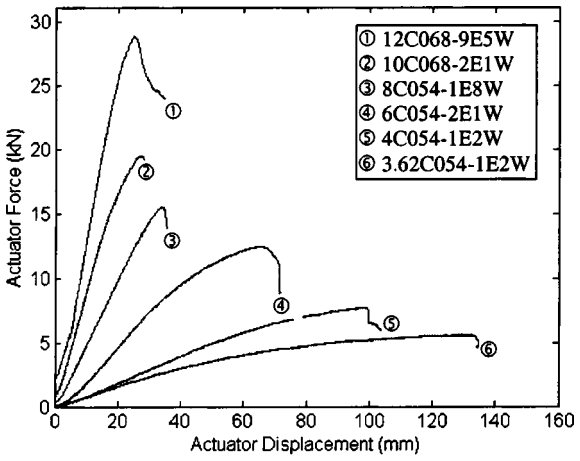

Fig. 16. Actuator force–displacement response for tests of 92–205 mm (3.62–12 in.) nominal deep *C*'s

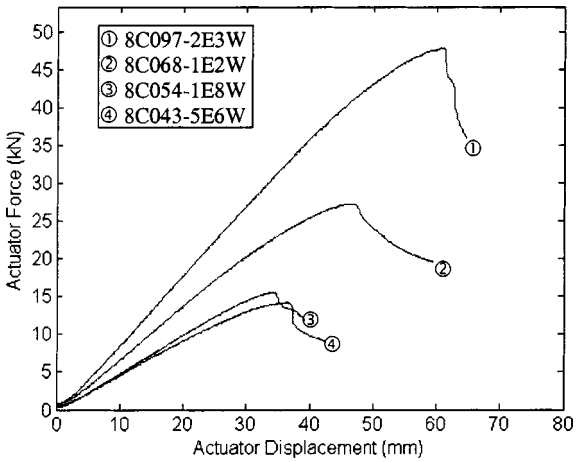

Fig. 15. Actuator force– displacement response for tests of 203 mm (8 in.) nominal deep *C*'s

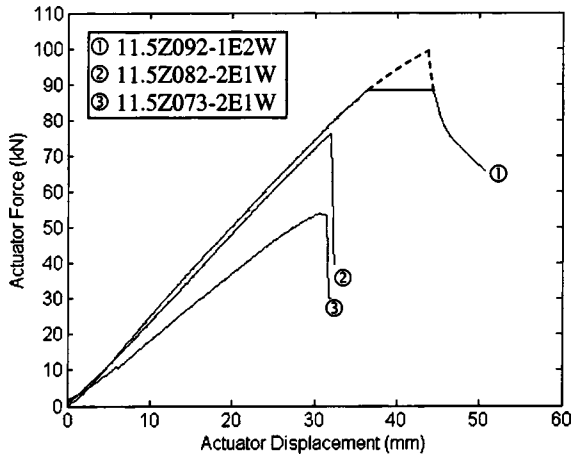

Fig. 17. Actuator force–displacement response for tests of 292 mm (11.5 in.) nominal deep *Z*'s

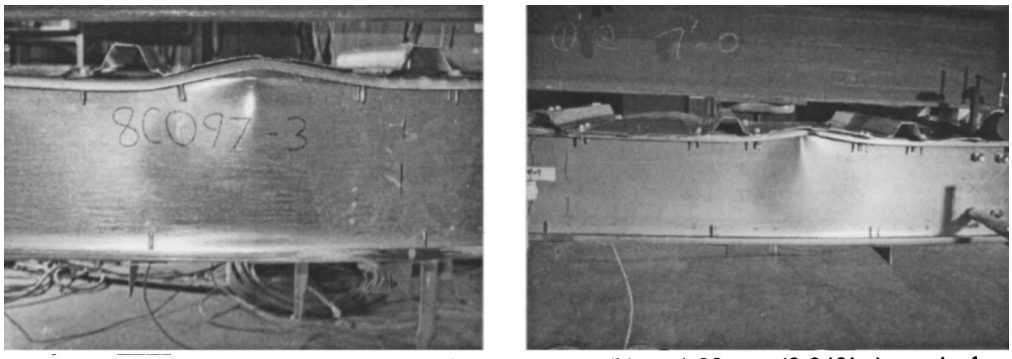

(a) t=2.46 mm (0.097 in.) nominal (test 8C097-2E3W)

(b) t=1.09 mm (0.043in.) nominal (test 8C043-5E6W)

Fig. 18. Observed failure mechanisms for tests on 203 mm (8 in.) nominal deep *C*'s

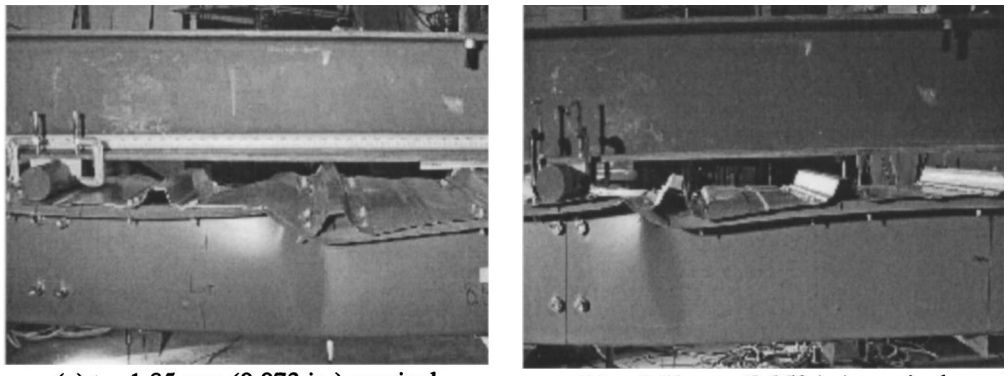

(a) t = 1.85 mm (0.073 in.) nominal (test 8.5Z073-4E3W)

(b) t=1.50 mm (0.059 in.) nominal (test 8.5Z059-4E3W)

Fig. 19. Collapse of 216 mm (8.5 in.) nominal deep *Z*'s

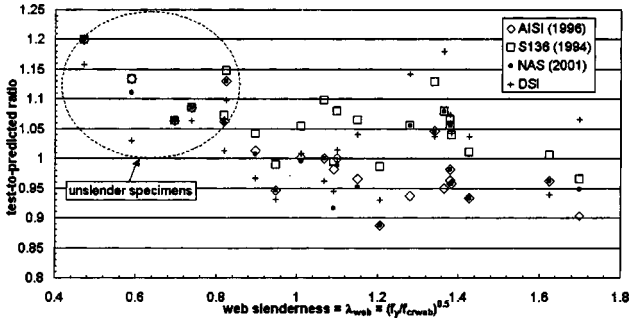

Fig. 20. Test-to-predicted ratios versus web slenderness

ment for M_{DSl} is quite good, additionally an examination of Fig. 20 shows that M_{DSl} is a fundamentally different method than AISI, S136, or NAS—and follows different trends as a function of web slenderness. For members with $\lambda_{web}<1.1$ M_{DSl} generally provides higher strength predictions than AISI, S136, or NAS, but as web slenderness increases to $\lambda_{web}>1.3$ this changes and M_{DSl} generally provides lower strength predictions than the conventional methods.

Web Effective Width

Assuming that the expressions for the effective width of flanges in AISI, S136, and NAS are accurate (they use nearly identical methods for flange effective width), then the experimentally observed capacity can be used to backcalculate the correct effective width for the web, expressed as $(b_1+b_2)/b_{comp}$, where b_1 and b_2 are the effective width of the compressive portions of the web, and b_{comp} is the depth of the full compression portion of the web (Fig. 21). The results of this calculation are given in Fig. 22. Neither AISI nor S136 provide an exact match to the data, but rather appear to provide somewhat reasonable bounds.

Conclusions

Through computational and experimental means, the developed testing plan and details have been shown to adequately restrict distortional buckling and provide a simple repeatable test that generates the local buckling flexural capacity for *C* and *Z* sections. Overall the test results indicate that AISI (1996), S136 (1994), and the new NAS (2001) design methods provide adequate strength predictions. However, the overall agreement is slightly skewed by a number of quite conservative predictions for unslender members that had observable inelastic reserve capacity ($M_{test}/M_y>1$). Among the considered methods, the direct strength method provides the best test-to-predicted ratio for both slender and unslender specimens. The test results demonstrate that many improvements in the elastic buckling and effective width calculation of *C*'s and *Z*'s are still possible. The authors intend to pursue additional testing and analysis to investigate the distortional buckling capacity of *C*'s and *Z*'s as well as more closely define the role of fasteners and other details.

Table 4. Summary of Test-to-Predicted Ratios for Existing and Proposed Design Methods

		Average (μ)					Standard deviation (σ)				
		M_{test}/M_{AISI}	M_{test}/M_{S136}	M_{test}/M_{NAS}	M_{test}/M_{DSl}	M_{test}/M_{DSd}	M_{test}/M_{AISI}	M_{test}/M_{S136}	M_{test}/M_{NAS}	M_{test}/M_{DSl}	M_{test}/M_{DSd}
Unslender $N=6$	Controlling	1.11	1.12	1.11	1.07	1.22	0.05	0.05	0.05	0.05	0.06
	Second	1.09	1.09	1.09	1.05	1.21	0.06	0.06	0.06	0.06	0.05
Slender $N=15$	Controlling	0.97	1.04	0.98	1.02	1.25	0.04	0.04	0.05	0.07	0.08
	Second	0.96	1.04	0.98	1.03	1.25	0.05	0.06	0.07	0.07	0.08
Overall	Controlling	1.01	1.06	1.02	1.03	1.24	0.04	0.04	0.05	0.06	0.07
	Second	1.00	1.05	1.01	1.04	1.24	0.05	0.06	0.07	0.07	0.07

Note: Slender: the specimens with $M_{test}/M_y<1.0$ (total $N=15$ tests). Unslender: The specimens with $M_{test}/M_y>=1.0$ (total $N=6$ tests). Controlling: The controlling specimens with panel type C or D. Second: the uncontrolling specimen of the paired set. M_{AISI}: AISI (1996) predicted flexural capacity. M_{S136}: S136 (1994) predicted flexural capacity. M_{NAS}: NAS (2001) predicted flexural capacity. M_{DSl}: direct strength–local mode expression as reported in Schafer (2002b) to AISI (a.k.a: M_{n1}). M_{DSd}: direct strength–distortional mode expression as reported in Schafer (2002b) to AISI (a.k.a: M_{nd}).

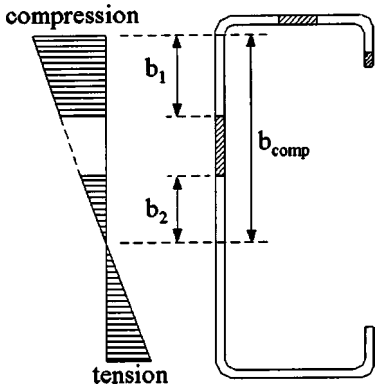

Fig. 21. Webs under stress gradient

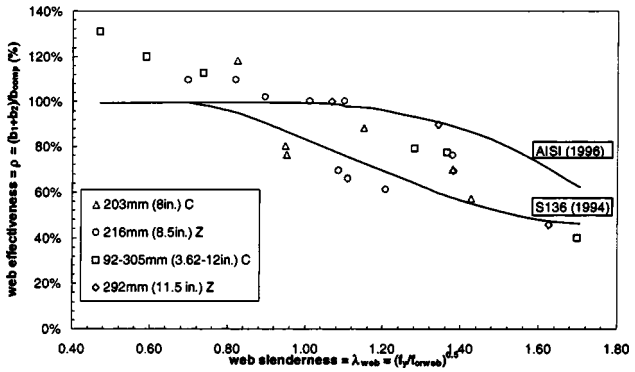

Fig. 22. Backcalculated experimental web effective widths versus predictions

Acknowledgments

The sponsorship of AISI and the Metal Building Manufacturers Association and the donation of materials by VP Buildings, and Clark Steel is gratefully acknowledged. The assistance of the AISI task group in developing the testing plan is appreciated. Don Johnson, Maury Golovin, Joe Nunnery, Joe Wellinghoff, and Steve Thomas have all been helpful with their ideas and generous with their time. Johns Hopkins undergraduates: Sam Phillips, Liakos Ariston, and Andrew Myers have provided additional support in the lab and deserve recognition as well. The assistance of Jack Spangler in reinvigorating the JHU structural testing facility has been invaluable. The donation of steel parts by Prosser Steel is also appreciated.

Notation

The following symbols are used in this paper:

b = flange width;
b_c = out-to-out compression flange width;
b_{comp} = the depth of the full compression portion of the web;
b_t = out-to-out tension flange width;
b_1, b_2 = the effective width of the compressive portions of the web;
d = flange lip width;
d_c = out-to-out compression flange lip stiffener length;
d_t = out-to-out compression flange lip stiffener length;
E = modulus of elasticity;
h = out-to-out web depth;
f_{cr} = critical buckling stress;
f_u = ultimate stress capacity;
f_y = yield stress;
M_{AISI} = AISI (1996) predicted flexural capacity;
M_{crd} = elastic critical distortional buckling moment;
M_{crl} = elastic critical local buckling moment;
M_{DSd} = direct strength–distortional mode expression;
M_{DSl} = direct strength–local mode expression;
M_{NAS} = NAS (2001) predicted flexural capacity;
M_{S136} = S136 (1994) predicted flexural capacity;
M_{test} = tested flexural capacity;
M_y = yield moment;
r_{dc} = outer radius between compression flange and lip;
r_{dt} = outer radius between tension flange and lip;
r_{hc} = outer radius between web and compression flange;
r_{ht} = outer radius between web and tension flange;
t = base metal thickness;
θ_c = compression flange stiffener angle from horizontal;
θ_t = tension flange stiffener angle from horizontal; and
λ_{web} = $(f_y/f_{cr})^{0.5}$, slenderness factor.

References

American Iron Steel Institute (AISI). (1996). ''Specification for the design of cold-formed steel structural members.'' American Iron and Steel Institute. Washington, D.C.

American Society for Testing and Materials (ASTM). (2000). ''E8-00, Standard test methods for tension testing of metallic material.'' *E8-00*,

American Society for Testing and Materials, Philadelphia, Pa.
Canadian Standards Association (1994). ''Cold-formed steel structural members.'' *S136-94*, Canadian Standards Association, Rexdale, Ont.
Elhouar, S., and Murray, T. M. (1985). ''Adequacy of proposed AISI effective width specification provisions for *Z*- and *C*-purlin design.'' Fears Structural Engineering Laboratory, *FSEL/MBMA 85-04*, University of Oklahoma, Norman, Okla.
HKS. (2001). *ABAQUS* Version 5.2., Hibbitt, Karlsson, and Sorensen, Inc., Pawtucket, R.I. ⟨www.hks.com⟩ (March 2002).
North American Specification (NAS). (2001). ''North American specification for the design of cold-formed steel structural members.'' American Iron and Steel Institute, Washington, D.C.
Schafer, B. W. (2001). ''*CUFSM* 2.5—Elastic buckling analysis of thin-walled members using the classical finite strip method: Users manual and tutorials.'' ⟨www.ce.jhu.edu/bschafer/cufsm⟩ (March 2002).
Schafer, B. W. (2002a). ''Local, distortional, and euler buckling in thin-walled columns.'' *J. Struct. Eng.*, 128(3), 289–299.
Schafer, B. W. (2002b). ''Design manual for direct strength method of cold-formed steel design.'' *Rep. to the American Iron and Steel Institute*, Washington, D.C.; available online at ⟨www.ce.jhu.edu/bschafer/direct_strength⟩ (March 2002).
Schafer, B. W., and Peköz, T. (1998). ''Direct strength prediction of cold-formed steel members using numerical elastic buckling solutions.'' *Proc., 14th Int. Spec. Conf. on Cold-Formed Steel Structures*, St. Louis., University of Missouri-Rolla, Rolla, Mo.
Schafer, B. W., and Peköz, T. (1999). ''Laterally braced cold-formed steel flexural members with edge stiffened flanges.'' *J. Struct. Eng.*, 125(2), 118–127.
Schafer, B. W., and Trestain, T. (2002). ''Interim design rules for flexure in cold-formed steel webs.'' *Proc., 16th Int. Spec. Conf. on Cold-Formed Steel Structures*, Orlando, Fla., University of Missouri-Rolla, Rolla, Mo.